Journal Pre-proof



Cellular-Level Assessment of Macular Development in Patients with FEVR Using Multimodal Imaging: A Prospective Cohort Study

Yarou Hu , Xinyu Zhao , Yaling Liu , Zhen Yu , Kaixuan Cui , Zhenquan Wu , Ziying Zhou , Ruiheng Zhang , Li Dong , Wenbin Wei , Shaochong Zhang , Wei Chi , Jie Zhang , Peiquan Zhao , Guoming Zhang

PII: S0002-9394(25)00510-0
DOI: https://doi.org/10.1016/j.ajo.2025.09.036
Reference: AJOPHT 13598

To appear in: *American Journal of Ophthalmology*

Received date: June 25, 2025
Revised date: September 20, 2025
Accepted date: September 20, 2025

Please cite this article as: Yarou Hu , Xinyu Zhao , Yaling Liu , Zhen Yu , Kaixuan Cui , Zhenquan Wu , Ziying Zhou , Ruiheng Zhang , Li Dong , Wenbin Wei , Shaochong Zhang , Wei Chi , Jie Zhang , Peiquan Zhao , Guoming Zhang , Cellular-Level Assessment of Macular Development in Patients with FEVR Using Multimodal Imaging: A Prospective Cohort Study, *American Journal of Ophthalmology* (2025), doi: https://doi.org/10.1016/j.ajo.2025.09.036

This is a PDF file of an article that has undergone enhancements after acceptance, such as the addition of a cover page and metadata, and formatting for readability, but it is not yet the definitive version of record. This version will undergo additional copyediting, typesetting and review before it is published in its final form, but we are providing this version to give early visibility of the article. Please note that, during the production process, errors may be discovered which could affect the content, and all legal disclaimers that apply to the journal pertain.

© 2025 Published by Elsevier Inc.

HIGHLIGHTS:

- Patients with FEVR without FH showed unvaried FAZ area but irregular FAZ morphology
- Patients with FEVR may be characterized by lower foveal but higher parafoveal cone densities
- Cone distribution changes in young patients with FEVR had no significant impact on BCVA
- Patients with vision loss may still have cone abnormalities despite exhibiting normal macular outlines.
- AO imaging can be quantitative and sensitive in exploring photoreceptor disorders

Journal Pre-proof

Cellular-Level Assessment of Macular Development in Patients with FEVR Using Multimodal Imaging: A Prospective Cohort Study

YAROU HU[a]*, XINYU ZHAO[b]*, YALING LIU[b], ZHEN YU[b], KAIXUAN CUI[b], ZHENQUAN WU[b], ZIYING ZHOU[b], RUIHENG ZHANG[c], LI DONG[c], WENBIN WEI[c], SHAOCHONG ZHANG[b], WEI CHI[b], JIE ZHANG[d], PEIQUAN ZHAO[e]*, AND GUOMING ZHANG[b,a]*

AFFILIATIONS:

[a] Shenzhen Eye Hospital, Jinan University, China.

[b] Shenzhen Eye Hospital, Shenzhen Eye Medical Center, Southern Medical University, Shenzhen, China.

[c] Beijing Tongren Eye Center, Beijing Key Laboratory of Intraocular Tumor Diagnosis and Treatment, Beijing Ophthalmology & Visual Sciences Key Lab, Medical Artificial Intelligence Research and Verification Key Laboratory of the Ministry of Industry and Information Technology, Beijing Tongren Hospital, Capital Medical University, Beijing, China.

[d] Advanced Ophthalmology Laboratory (AOL), Robotrak Technologies, Nanjing, China

[e] Xinhua Hospital affiliated to Shanghai Jiao Tong University School of Medicine, Shanghai, China.

* Yarou Hu and Xinyu Zhao contributed equally as co-first authors, Guoming Zhang and

Journal Pre-proof

Peiquan Zhao contributed equally as co-senior authors.

SHORT TITLE: Cellular-level features of macula in patients with FEVR

CORRESPONDING AUTHOR: Guoming Zhang, Shenzhen Eye Hospital, Shenzhen Eye Medical Center, Southern Medical University, 18 Zetian Road, Futian District, Shenzhen, 518040, China. E-mail: zhangguoming@sz-eyes.com. ORCID: 0000-0003-2123-8125

Peiquan Zhao, Xin Hua Hospital Affiliated to Shanghai Jiao Tong University School of Medicine, 1665 Kongjiang Road, Shanghai, 200092, China. E-mail: zhaopeiquan@126.com.

Journal Pre-proof

ABSTRACT

PURPOSE: To investigate the multimodal characteristics of macula in patients with familial exudative vitreoretinopathy (FEVR) at a cellular level.

DESIGN: Prospective cohort study.

PARTICIPANTS: A total of 46 FEVR-affected and healthy eyes were enrolled from July to October 2024 and underwent multimodal examinations. Participants with conditions such as foveal hypoplasia (FH), a history of ocular surgery or trauma in both the control and FEVR groups were excluded.

METHODS AND MAIN OUTCOME MEASURES: All participants were underwent examinations of scanning laser ophthalmoscopy (SLO), ultra-wide-field swept source optical coherence tomography angiography (UWF SS-OCTA), and adaptive optics (AO)-SLO to acquire metrics of multimodal macular characteristics such as macular appearance, layered structure, vasculature and photoreceptor distribution. The baseline information such as best-corrected visual acuity (BCVA), spherical equivalent (SE), and axial length (AL) were also measured.

RESULTS: Comparing to age (9.76 years on average), gender (52% femal), SE (-1.01D on average) and AL (23.66mm on average)-matched healthy eyes, FEVR-affected eyes without FH had increased foveal avascular zone (FAZ) perimeter in deep capillary plexus (DCP), partly thickening inner retina layers and thinning outer nuclear layer, as well as partly lower vessel density of DCP ($P<0.05$). In cellular-level, eyes with FEVR showed numerically lower cone density and larger cone spacing in fovea, but significantly higher cone density ($P=0.03$) and smaller cone spacing ($P=0.02$) in parafovea, as well as higher cone dispersion and lower regularity ($P<0.05$). Foveal and parafoveal cone density in participants with low BCVA were numerically higher.

CONCLUSIONS: Patients with FEVR without FH may be characterized by irregular FAZ morphology and cone distribution, exhibiting lower foveal and higher parafoveal cone densities, which was not correlated with their BCVA and may serve as clinical biomarkers for diagnostic assistance in FEVR. Participants with low BCVA but morphologically normal macular structure may harbor underlying cone abnormalities, underscoring the

Journal Pre-proof

necessity for more thorough assessment, warranting greater caution in diagnosing amblyopia until excluding the influence of cellular-level abnormalities.

KEYWORDS: Familial exudative vitreoretinopathy; Multimodal imaging; Foveal avascular zone; Adaptive optics; Cone density; Retinal thickness.

INTRODUCTION

Macular development, particularly the development of the fovea, is essential for maintaining the structural and functional integrity of human retina, as it directly impacts visual performance.[1] Foveal hypoplasia (FH) is a congenital retinopathy characterized by arrested development or complete absence of macular fovea, frequently associated with reduced visual acuity (VA). This condition can occur in isolation or in conjunction with other diseases,[2] with familial exudative vitreoretinopathy (FEVR) being a notable example of the latter.[3]

FEVR is an inherited eye disease characterized by abnormalities of retinal vascular development.[4] It can present as retinal detachment (RD) in children,[5] and is also associated with arrested development of the macula (showing as FH)[6,7] and even of the whole eye.[8] While significant attention has been directed toward comorbidities such as RD and FH, both of which can result in macular anomalies with reduced best corrected VA (BCVA) in patients with FEVR have received a lot of attention,[5-7] a considerable number of patients with FEVR who do not exhibit overt macular dysplasia or

complications remained understudied, with their vision loss often simply attributed to amblyopia.[9,10]

To date, the specialization of photoreceptors and the relationships among macular structure, photoreceptor morphology, and visual function in patients with FEVR remain unclear. The existing knowledge gaps, combined with the necessity to elucidate the underlying causes of vision loss, underscore the importance of studying macular photoreceptor morphology and function in patients with FEVR. Although some prior studies have examined the distribution of macular photoreceptors in both healthy[11-13] and amblyopic eyes[14,15], they have often lacked of comprehensive analyses of visual function, ocular biometric characteristics, retinal thickness, retinal blood flow and fundus photography.

To address these gaps, we conducted a cohort study that recruited healthy participants and patients with FEVR without comorbid FH. Using multimodal imaging, our objective was to explore macular development at a cellular level, with a focus on photoreceptor specialization, structure-functional correlations, and the underlying pathogenesis of vision loss in both patients with FEVR and participants experiencing vision loss.

METHODS

This cohort study was conducted at Shenzhen Eye Hospital (SZEH) and received approval from the Medical Ethics Committee of SZEH (2023KYPJ006) prior to its

Journal Pre-proof

initiation. The participants' parents provided informed consent for their children to participate. This study also complies with the principles of Declaration of Helsinki and the requirements of HIPAA on the management of patient health information.

PARTICIPANTS RECRUITMENT AND EXAMINATIONS

Participants were managed through the Eyecare-cloud platform,[16] a longitudinal cohort database comprising over 200 families affected by FEVR, enrolled since 2004. Building on this cohort, we conducted the present study, prospectively enrolling 15 eyes from 12 patients with FEVR (FEVR group) and 31 healthy eyes from 20 participants (control group) between July and October 2024, who were also managed on this platform. Eyes with low BCVA, defined as below age-matched normative values, were classified as group A for both FEVR and control groups. Eyes with normal BCVA were categorized as group B for the FEVR group and group C for the control group.

The inclusion criteria for the FEVR group were as follows: (1) eyes diagnosed with FEVR based on FFA or ultra-wide-field swept source optical coherence tomography angiography (UWF SS-OCTA), aligned with the diagnostic standard of our previous study;[8] (2) FEVR without FH (patients with FH were also excluded for their poor fixation during examing), macular or disc dragging, retinal detachment, and retinal folds. The inclusion criteria for control group were as follows: (1) eyes without any ocular diseases, including healthy eyes in patients with conditions that do not affect both eyes, such as Coats' disease, persistent fetal vasculature (PFV) and morning glory syndrome (MGS), as well as the absence of any systemic diseases that could impact ocular development;

(2) absence of FH. Common exclusion criteria for both groups were as follows: (1) a history of ocular surgery or trauma; (2) inability to cooperate with the examinations; (3) unavailability of measurement data and poor-quality images.

Participants underwent assessments of vision, optometry, and biometrics to acquire basic characteristics. The primary metrics of macular development were measured using apparatus of scanning laser ophthalmoscopy (SLO) (Optos 200Tx, Optos PLC, Scotland, UK), UWF SS-OCTA (BM-400K BMizar, TowardPi Medical Technology, Beijing, China), and adaptive optics (AO)-SLO (Mona IIa; Robotrak Technologies, Nanjing, China).

All examinations for each participant were conducted within a single day. During data processing, two ophthalmologists YRH and XYZ were responsible for the review and calibration of all images and measurement data to ensure the clear image quality, accurate positioning, precise image segmentation, and data analysis.

Journal Pre-proof

ACQUISITION OF BASIC OCULAR CHARACTERISTICS

Visual Acuity

All participants underwent VA testing to obtain BCVA with cycloplegic refraction (as follows). Measurements of BCVA were recorded using a Snellen Chart and subsequently converted into logarithm of the minimum angle of resolution (logMAR) values.

Refraction

The refraction examinations were conducted by optometrists with over 10 years of experience. Participants' pupils were dilated to 6mm using 0.5% tropicamide,

administered three times at 5- to 10-minutes intervals. Following dilation, participants were taken into a dark room for retinoscopy.

Biometrics

Ocular biometric characteristics were measured using IOLMaster 700 (Carl Zeiss Meditec AG, Jena, Germany) to obtain axial length (AL), which is a confounding factor to be eliminated, as prior studies have indicated that the cone density may vary with increasing AL.[17-18]

ACQUISITION OF MAIN METRICS ON MACULAR ASSESSMENT

SLO Image Capture and Analysis

All participants underwent multi-orientation fundus imaging using SLO, capturing images from central (C), superior (S), inferior (I), nasal (N), and temporal (T) orientations. This approach ensured that patients with FEVR exhibited characteristic diagnostic features, such as peripheral retinal avascular zones, while participants in the control group displayed a full vascularized and healthy retina. In addition, SLO images were used to visualize the macular morphology, including features such as the foveal reflex.

UWF SS-OCTA Image Capture and Analysis

UWF SS-OCTA images were captured by a technician with over 10 years of experience. The instrument performs full-layer scans of retinal areas approximately $20\times24mm^2$ with automatic feature segmentation. To focus on the macular assessment, we employed the build-in measure tool, specifically the Early Treatment Diabetic

Journal Pre-proof

Retinopathy Study (ETDRS) grid for macular zoning (shown in Figure 1), which consists of three concentric circles with diameters of 1, 3, and 6mm. The inner circle is isolated (mainly covering the fovea), while the inner ring (mainly covering the parafovea) and outer ring (mainly covering the perifovea) are each divided into four subfields — S, I, N, and T, labeled as C, inner-S, inner-I, inner-N, inner-T, outer-S, outer-I, outer-N and outer-T, respectively.

We analyzed retinal feature parameters of retinal thickness (analysis mode ①in Figure 1) and retinal blood flow (analysis mode ②in Figure 1), and measured their average values across the nine subfields, including the foveal center, within designated retinal layers. Retinal thickness values (μm) were converted into percentage (%) of the retinal layers relative to the whole retina slab. Additionally, the area (mm^2) and perimeter (mm) of the foveal avascular zone (FAZ) were recorded.

AO-SLO Image Capture and Analysis

AO-SLO imaging system is equipped with ancillary analytic software that facilitates not only images capture but also automated cone segmentation and quantitative analysis. This system generates metrics such as cone density, spacing, dispersion and regularity. Cone density refers to the number of cells per unit area (mm^2), while cone spacing denotes the average distance between adjacent cells. Cone dispersion is calculated as mean cell distance divided by variance, indicating the consistency or spread of cellular distribution. Cone regularity reflects the homogeneity of cellular density.

Among the scanning modes available, we selected the medium mode of 2.4°×2.4° (approximately equivalent to 700×700μm^2 in retinal area) as the standardized protocol. During imaging, participants sequentially fixated on the C, S, I, N, and T orientations (3° eccentricity from the foveola), and repeating the imaging process until high-quality retinal images were obtained. Each peripheral image spanned a range of 1.8°~4.2° (approximately 550~1250μm), primarily covering the parafovea, while central images covered 0°~1.2° eccentricity, focusing on the fovea.

To account for limited resolution in foveola, we used a built-in tool with a diameter of 300μm (represented as the smaller circles in Figure 2 E~F) to exclude foveolar data from central images, and recorded as whole-300. Adjacent regions of foveola were further analyzed using measurement tools with side lengths of 50μm or 80μm (represented as squares in Figure 2 E~F). The average values from boxes with similar eccentricities were calculated and labeled as inner/middle/outer-50 and inner/outer-80. (for example, inner-50 was calculated as mean of the eight inner 50μm squares)

Journal Pre-proof

STATISTICAL ANALYSIS

Statistical analyses were performed using SPSS 23.0 software (SPSS, Inc., Chicago, IL, USA). Continuous variables were presented as mean ± standard deviation (*SD*), while categorical variables were presented as counts and percentages. Independent samples t test and Mann-Whitney U test (for non-normally distributed data) were used for comparisons of continuous variables. Comparisons between categorical variables were

conducted using Pearson's chi-square test. A p-value of less than 0.05 was considered statistically significant.

RESULTS

BASIC CHARACTERISTICS OF PARTICIPANTS

There were no significant difference in basic characteristics, including age, gender, spherical equivalent (SE), and AL, between FEVR and control groups. (Table 1) In the FEVR group, 66.7% patients (8/12) underwent genetic testing, while 25.0% (2/8) tested positive for FEVR-associated genes. Both the patients carried a heterozygous missense variant in the ZNF408 gene (autosomal dominant inheritance, located on chromosome 11, uncertain clinical significance by ACMG criterion: PM2. In the control group, four out of 31 eyes were from healthy eyes of participants with unilateral eye disease, including two cases with Coats' disease, one case with PFV, and one case with MGS.

Among all participants, we identified four out of 46 eyes from four individuals (participants A~D in Table 1) with BCVA below age-matched normative values, with BCVA values of 0.50, 1.00, 0.70, and 0.50, respectively. Participant A was a patient with FEVR in the FEVR group, while participants B~D were from the control group. Participants B and C were healthy individuals with symmetrical bilateral refraction, and participant D had MGS in the fellow eye.

SLO OBSERVATION ON MACULAR MORPHOLOGY

Journal Pre-proof

SLO images of all participants, including those with low BCVA (group C), showed a normally appearing macula characterized by the presence of foveal reflexes (Figure 3). Except for the patients with FEVR, all other participants exhibited healthy peripheral retinas without any fundus lesions.

UWF SS-OCTA ASSESSMENT ON MACULAR STRUCTURE AND VASCULATURE

Macular Fovea (within 1mm)

Transverse scan images showed normally developed macular foveas (a wide and deep foveal pit) in all eyes (Figure 4 A~F). Correspondently, there were no significant differences in thicknesses of inner retina layers (IRLs) (P=0.16), outer nuclear layer (ONL) (P=0.35), photoreceptor layer (PL) (P=0.18), and the whole retina slab (P=0.19) in C subfield, as well as in the foveal center (P=0.21), between FEVR and control groups (Table 2, Figure 5).

Comparing to group A and C, eyes with FEVR in group B showed FAZ morphology manifested as a highly asymmetrical irregularly polygon with distorted edge, particularly in the deep capillary plexus (DCP) (Figure 4 G~I). This phenomenon accounted for the significant difference in FAZ perimeter of DCP (P=0.046) betwen FEVR and control groups (Table 2). However, there was no significant differences in FAZ areas or retinal vessel density in C subfield.

Macular Parafovea and Perifovea (1-3-6mm)

The quantitative measurements around the fovea were less consistent between the

Journal Pre-proof

two groups compared to those in the fovea. (Table 2, Figure 5) In the FEVR group, the retinal thickness of IRLs were found to be thicker in the inner-I (P=0.045) and inner-T (P=0.03) subfields, whereas ONL in the inner-T (P=0.03) subfield was thinner. (Table 3, Figure 5) Except for the lower vessel density in DCP in the inner-N (P=0.02) and outer-S (P=0.04) subfields in the FEVR group, no other significant difference in retinal vessel density of subfields peripheral to the fovea were observed between the two groups. (Table 3, Figure 5)

AO-SLO ANALYSIS ON MACULAR PHOTORECEPTOR DISTRIBUTION

Macular Fovea (central image)

As shown in Table 4, there were no significant difference in foveal cone density, spacing and dispersion between FEVR and control groups. However, when compared to control group, FEVR group exhibited significantly lower overall foveal cone regularity (P=0.02), particularly in regions further from the foveola (outer-50 and outer-80: P=0.03, P=0.04, respectively).

As shown in Figure 6, eyes with FEVR in group B (dark red in image D'~F' correspondIing to 5.2~7.3e+04/mm^2) demonstrated visibly lower foveal cone density and a slower rate of decrease towards periphery compared to healthy eyes in group C (dark red in image G'~I' corresponds to 7.7~8.4e+04/mm^2). In fact, the lower cone density, higher cone spacing, and slower decrease of cone density in eyes with FEVR were evident across all regions of fovea from the numeric data in Table 4.

Journal Pre-proof

Macular Parafovea (peripheral images with 3° eccentricity)

Conversely, peripheral data showed that the average cone density at the four parafoveal orientations was statistically significantly higher (P=0.03), while cone spacing was significantly lower (P=0.02) in the FEVR group compared to the control group, with these differences observed at almost all orientations (Table 5).

There may be differences in parafoveal cone dispersion (I: P=0.04, T: P=0.06) and regularity (S: P=0.06, T: P=0.06) between FEVR and control groups, similar to those found in fovea. Nevertheless, eyes with FEVR maintained over 95% regular cone arrangement in both fovea and parafovea. In Figure 6, similar to the fovea, the representative eye with FEVR from group B showed higher cone density in the parafovea (dark red in image K'1~4, corresponding to 3.6~4.5e+04/mm^2) compared to the healthy eye in group C (dark red in image L'1~4, corresponding to 3.0~4.2e+04/mm^2).

Cone Analysis on Participants with Low BCVA

In the fovea, the average cone density in eyes with low BCVA (group A) was 48895.77, 50338.62 and 47709.68 at the inner, middle, and outer-50 positions, respectively; 49389.60 and 48088.73 at the inner and outer-80 positions; and 44533.14 at the whole-300 position (/mm^2). These measurements were observed to be higher than those in eyes of group C (47513.09, 46608.05 and 45526.23; 45139.14 and 45660.55; 44034.05; /mm^2).

In the parafovea, compared to eyes of group C, the average cone density at the four

Journal Pre-proof

orientations in group A was also higher (22131.22±1272.06 vs 21772.56±2524.00; /mm^2), and cone spacing was lower (5.57±0.34 vs 5.67±0.45; μm).

DISCUSSION

This study utilized multimodal imaging techniques to elucidate the appearance, layered structure and vasculature, and photoreceptor distribution in the macula, thereby providing novel insights into macular development in patients with FEVR. Both SLO and UWF SS-OCTA images demonstrated nearly normal manifestation. Several key findings emerged:

1) Photoreceptor anomalies: eyes with FEVR exhibited numerically lower foveal cone density and increased cone spacing, increased significantly higher parafoveal cone density (P=0.03) and reduced cone spacing (P=0.02). Irregular cone distribution was also noted (P<0.05), while the retinal thickness of PL in both the fovea (foveal center and C subfield) and parafovea (inner ring) were comparable to control group. 2) Vascular features: patients with FEVR displayed irregular DCP-FAZ morphology with increased perimeter (P=0.046). 3) Layered structural changes: There was a tendency for thickening IRLs and thinning ONL (inner-T and inner-I) in parafovea, as well as lower vessel density of DCP (inner-N and outer-S). (P<0.05)

Few AO imaging studies have specifically examined the distribution of cone photoreceptor in patients with FEVR. We hypothesize that the inverted changes in foveal-parafoveal density may stem from genetic mutations or arrested foveal maturation

(disrupting central cone migration), consistent with the hallmark developmental arrest phenotype[6-8,19] associated with FEVR. Notably, our OCTA results indicated reduced vessel density of DCP in non-FH patients with FEVR, consistent with observations by Ding et al.6 and complementing theirs. While their study reported a smaller FAZ and perimeter in the FH cases, we identified an irregular FAZ with a larger perimeter in non-FH cases — mechanisms underlying the differences warrant further investigation.

It is well established that cone density[20,21] and visual resolution[11] decline rapidly with increasing eccentricity from the fovea. Intriguingly, 14 of 15 FEVR-affected eyes with abnormal cone gradients maintained normal BCVA despite reductions in foveal cone density. This paradox may be explained by several factors: 1) Cone functional redundancy: prior studies have demonstrated that a decrease in cone density within certain limits has minimal impact on vision and is not linearly correlated with vision.[22,23] It has been reported that better BCVA (≥ 20/12.5) is associated with higher cone density,[24] but the majority (11 of 12) of patients with FEVR in this study were under 13 years old, and their ultimate BCVA remains unknown.1,[25] 2) Subclinical changes: the observed reductions in foveal density (P>0.05) may be insufficient to affect visual acuity. 3) Unidentified impacts: increase in cone density among patients with FEVR may affect the visual function other than VA.

It's noteworthy that the cone density in the eyes with low BCVA appeared to increase in both the fovea and parafovea. However, this observation contrasts with findings of Sharma et al.15, which reported decreased cone density in isoametropic

amblyopia. The difference may result from varying causes of developing amblyopia in the two samples, as only two participants with low BCVA had symmetzrical bilateral refraction in our study. Due to the limited sample size, we did not performed formal statistical comparisons between low BCVA and control eyes. Therefore, we cannot entirely exclude chance occurrence due to the small sample size. Besides, the increase in overall cone density in eyes with low BCVA was slight, potentially aligning with the study by Liao et al.14 who found no significant difference between participants with and without amblyopia.

In summary, AO imaging may be essential for exploring macular microstructure disorder and photoreceptor characteristics. Key advantages include: 1) Microscale resolution: While foveal OS thickness is only four times greater than that of perifoveal regions25, foveal peak cone density exceeds that of periphery at 3°~6° eccentricity by over 100 times (2e+6 vs 1.5~2e+4/mm^2)16,19,[26-29], AO enabling the detection of cellular-level changes that are invisible to structural imaging. 2) Diagnostic potential: FEVR-specific patterns of reduced foveal cone density with blunted parafoveal gradient and irregular FAZ may serve as novel biomarkers. 3) Etiological insights: AO-SLO assists in identifying cone developmental anomalies in low BCVA cases, complementing existing FH grading systems that rely on subjective SD-OCT criteria[30], thereby presenting challenges for amblyopia diagnosis and necessitating more cautious judgment for participants with low BCVA.

LIMITATIONS

Journal Pre-proof

Firstly, this cohort study did not include measurements of visual function other than VA. Therefore, the correlation between cone distribution changes and overall visual function remains unspecified. In subsequent follow-ups, we plan to implement further examinations, including a comprehensive evaluation of visual function. Secondly, the sample size in this study was limited, particularly with regard to participants with low VA. While a larger cohort would be advantageous, it necessitates a longer duration for recruitment since FEVR was still regarded as a rare disease.[31,32] Nonetheless, we are pleased to report our novel findings from this prospective cohort study, which spanned only a few months and yielded results with both clinical significance and statistical difference in a sample of only 46 eyes. However, more detailed and comprehensive investigations are warranted, and we will proceed accordingly.

CONCLUSION

Patients with FEVR without FH may be characterized by irregular FAZ morphology and cone distribution, exhibiting lower foveal and higher parafoveal cone densities, which was not correlated with their BCVA and may serve as clinical biomarkers for diagnostic assistance in FEVR. Participants with low BCVA but morphologically normal macular structure may harbor underlying cone abnormalities, underscoring the necessity for more thorough assessment, warranting greater caution in diagnosing amblyopia until excluding the influence of cellular-level abnormalities.

Journal Pre-proof

CREDIT AUTHORSHIP CONTRIBUTION STATEMENT:

Yarou Hu: Conceptualization, Data curation, Formal analysis, Methodology, Software, Validation, Visualization, Writing – original draft. **Xinyu Zhao:** Conceptualization, Data curation, Methodology, Supervision, Validation, Funding acquisition, Writing – review and editing. **Yaling Liu:** Data curation, Methodology, Software, Validation, Writing – review and editing. **Zhen Yu, Kaixuan Cui and Zhenquan Wu:** Data curation, Methodology, Validation, Funding acquisition, Writing – review and editing. **Ziying Zhou:** Data curation, Software, Writing – review and editing. **Ruiheng Zhang, Li Dong and Wenbin Wei:** Data curation, Writing – review and editing. **Shaochong Zhang, Wei Chi and Jie Zhang:** Methodology, Writing – review and editing. **Peiquan Zhao:** Conceptualization, Supervision, Methodology, Project administration, Validation, Writing – review and editing. **Guoming Zhang:** Conceptualization, Supervision, Methodology, Project administration, Validation, Funding acquisition, Writing – review and editing.

ACKNOWLEDGEMENTS: The authors wish to express gratitude to all participants and their families for their support, as well as to the institutions that funded the projects for co-authors of this study. We also extend our appreciation to the Shenzhen Eye Hospital Medical Ethics Committee for approving the conduct of this study (2023KYPJ006). Yarou Hu and Xinyu Zhao contributed equally as co-first authors, Guoming Zhang and Peiquan Zhao contributed equally as co-senior authors.

Journal Pre-proof

Funding/Support: This work was supported by the National Natural Science Foundation of China (82271103, 82401315, 82301269, 82301226, 82401272); the Sanming Project of Medicine in Shenzhen (SZSM202311018); the Guangdong Basic and Applied Basic Research Foundation (2022A1515110865); the Shenzhen Medical Research Fund (C2301005, A2403020); the Shenzhen Key Medical Discipline Construction Fund (SZXK038); the Shenzhen Fund for Guangdong Provincial High level Clinical Key Specialties (SZGSP014); the Shenzhen Science and Technology R&D Fund Project (JCYJ20240813152703005, JCYJ20220530153607015); and the China Ophthalmology New Technology Incubation Project.

Financial Disclosures: The authors declare no financial disclosures.

Journal Pre-proof

REFERENCE

[1] Thomas MG, Papageorgiou E, Kuht HJ, et al. Normal and abnormal foveal development. Br J Ophthalmol. 2022 May;106(5):593-599. doi: 10.1136/bjophthalmol-2020-316348.

[2] Storp JJ, Zimmermann JA, Danzer MF, et al. Characterizing Foveal Hypoplasia Using Optical Coherence Tomography Angiography: Evaluation of Microvascular Abnormalities and Clinical Significance. J Clin Med. 2023 Jul 29;12(15):4992. doi: 10.3390/jcm12154992.

[3] Ju Y, Zhang L, Gao F, et al. Genetic Characteristics and Clinical Manifestations of Foveal Hypoplasia in Familial Exudative Vitreoretinopathy. Am J Ophthalmol. 2024 Jun;262:73-85. doi: 10.1016/j.ajo.2024.01.029.

[4] Zhu X, Yang M, Zhao P, et al. Catenin α 1 mutations cause familial exudative vitreoretinopathy by overactivating Norrin/β-catenin signaling. J Clin Invest. 2021 Mar 15;131(6):e139869. doi: 10.1172/JCI139869.

[5] Wang PP, Liu LQ. Primary Diseases of 393 Cases of Pediatric Retinal Detachment and the Distribution of Clinical Characteristics. Sichuan Da Xue Xue Bao Yi Xue Ban. 2021 Nov;52(6):1016-1021. doi: 10.12182/20211160305

[6] Chen C, Liu C, Wang Z, et al. Optical Coherence Tomography Angiography in Familial Exudative Vitreoretinopathy: Clinical Features and Phenotype-Genotype Correlation. Invest Ophthalmol Vis Sci. 2018 Dec 3;59(15):5726-5734. doi: 10.1167/iovs.18-25377.

[7] Yonekawa Y, Thomas BJ, Drenser KA, et al. Familial Exudative Vitreoretinopathy: Spectral-Domain Optical Coherence Tomography of the Vitreoretinal Interface, Retina, and Choroid. Ophthalmology. 2015 Nov;122(11):2270-7. doi: 10.1016/j.ophtha.2015.07.024.

[8] Hu Y, Fan Z, Zhao X, et al. Refractive Status and Biometric Characteristics of Children With Familial Exudative Vitreoretinopathy. Invest Ophthalmol Vis Sci. 2023 Oct 3;64(13):27. doi: 10.1167/iovs.64.13.27.

[9] Chen C, Guo S, Zhao R, et al. A boy with amblyopia and familial exudative vitreoretinopathy harboring a new mutation of LRP5 and OPA1: A case report. Front Genet. 2022 Sep 29;13:998846.

Journal Pre-proof

doi: 10.3389/fgene.2022.998846.

[10] Chang HH, Wang AG, Niu DM, et al. Unveiling novel LRP5 pathogenic variant in familial exudative vitreoretinopathy: Diverse phenotypic expressions in a mother-daughter duo. Eur J Ophthalmol. 2024 Sep;34(5):NP8-NP12. doi: 10.1177/11206721241254129.

[11] Rossi EA, Roorda A. The relationship between visual resolution and cone spacing in the human fovea. Nat Neurosci. 2010 Feb;13(2):156-7. doi: 10.1038/nn.2465.

[12] Tumahai P, Moureaux C, Meillat M, et al. High-resolution imaging of photoreceptors in healthy human eyes using an adaptive optics retinal camera. Eye (Lond). 2018 Nov;32(11):1723-1730. doi: 10.1038/s41433-018-0140-1.

[13] Cava JA, Allphin MT, Mastey RR, et al. Assessing Interocular Symmetry of the Foveal Cone Mosaic. Invest Ophthalmol Vis Sci. 2020 Dec 1;61(14):23. doi: 10.1167/iovs.61.14.23.

[14] Liao N, Jiang H, Mao G, et al. Changes in macular ultrastructural morphology in unilateral anisometropic amblyopia. Am J Transl Res. 2019 Aug 15;11(8):5086-5095.

[15] Sharma P, Anand M, Sharma A, et al. Evaluation of retinal function and morphology in isoametropic amblyopia. Indian J Ophthalmol. 2023 Jan;71(1):222-228. doi: 10.4103/ijo.IJO_1685_22.

[16] Zhao X, Wu Z, Liu Y, et al. Eyecare-cloud: an innovative electronic medical record cloud platform for pediatric research and clinical care. EPMA J. 2024 Jul 11;15(3):501-510. doi: 10.1007/s13167-024-00372-6.

[17] Legras R, Gaudric A, Woog K. Distribution of cone density, spacing and arrangement in adult healthy retinas with adaptive optics flood illumination. PLoS One. 2018 Jan 16;13(1):e0191141. doi: 10.1371/journal.pone.0191141.

[18] Woog K, Legras R. Distribution of mid-peripheral cones in emmetropic and myopic subjects using adaptive optics flood illumination camera. Ophthalmic Physiol Opt. 2019 Mar;39(2):94-103. doi: 10.1111/opo.12604.

[19] Ranchod TM, Ho LY, Drenser KA, et al. Clinical presentation of familial exudative vitreoretinopathy.

Ophthalmology. 2011 Oct;118(10):2070-5. doi: 10.1016/j.ophtha.2011.06.020.

[20] Curcio CA, Sloan KR, Kalina RE, et al. Human photoreceptor topography. J Comp Neurol. 1990 Feb 22;292(4):497-523. doi: 10.1002/cne.902920402.

[21] Wang X, Hoshi S, Liu R, et al. Modeling Human Macular Cone Photoreceptor Spatial Distribution. Invest Ophthalmol Vis Sci. 2024 Jul 1;65(8):14. doi: 10.1167/iovs.65.8.14.

[22] Bensinger E, Rinella N, Saud A, et al. Loss of Foveal Cone Structure Precedes Loss of Visual Acuity in Patients With Rod-Cone Degeneration. Invest Ophthalmol Vis Sci. 2019 Jul 1;60(8):3187-3196. doi: 10.1167/iovs.18-26245.

[23] Foote KG, Loumou P, Griffin S, et al. Relationship Between Foveal Cone Structure and Visual Acuity Measured With Adaptive Optics Scanning Laser Ophthalmoscopy in Retinal Degeneration. Invest Ophthalmol Vis Sci. 2018 Jul 2;59(8):3385-3393. doi: 10.1167/iovs.17-23708.

[24] Cheng H, Ciuffreda KJ, Jiang H, et al. Cone parameters in different vision levels from the adaptive optics imaging. Medicine (Baltimore). 2021 Apr 23;100(16):e25618. doi: 10.1097/MD.0000000000025618.

[25] Hendrickson A, Possin D, Vajzovic L, et al. Histologic development of the human fovea from midgestation to maturity. Am J Ophthalmol. 2012 Nov;154(5):767-778.e2. doi: 10.1016/j.ajo.2012.05.007.

[26] Domdei N, Ameln J, Gutnikov A, et al. Cone Density Is Correlated to Outer Segment Length and Retinal Thickness in the Human Foveola. Invest Ophthalmol Vis Sci. 2023 Dec 1;64(15):11. doi: 10.1167/iovs.64.15.11.

[27] Burns SA, Elsner AE, Sapoznik KA, et al. Adaptive optics imaging of the human retina. Prog Retin Eye Res. 2019 Jan;68:1-30. doi: 10.1016/j.preteyeres.2018.08.002.

[28] Dabir S, Mangalesh S, Kumar KA, et al. Variations in the cone packing density with eccentricity in emmetropes. Eye (Lond). 2014 Dec;28(12):1488-93. doi: 10.1038/eye.2014.229.

[29] Jackson K, Vergilio GK, Cooper RF, et al. A 2-Year Longitudinal Study of Normal Cone Photoreceptor Density. Invest Ophthalmol Vis Sci. 2019 Apr 1;60(5):1420-1430. doi:

10.1167/iovs.18-25904.

[30] Thomas MG, Kumar A, Mohammad S, et al. Structural grading of foveal hypoplasia using spectral-domain optical coherence tomography a predictor of visual acuity? Ophthalmology. 2011 Aug;118(8):1653-60. doi: 10.1016/j.ophtha.2011.01.028.

[31] Wang Z, Liu CH, Huang S, et al. Wnt Signaling in vascular eye diseases. Prog Retin Eye Res. 2019 May;70:110-133. doi: 10.1016/j.preteyeres.2018.11.008.

[32] Le V, Abdelmessih G, Dailey WA, et al. Mechanisms Underlying Rare Inherited Pediatric Retinal Vascular Diseases: FEVR, Norrie Disease, Persistent Fetal Vascular Syndrome. Cells. 2023 Nov 5;12(21):2579. doi: 10.3390/cells12212579.

Journal Pre-proof

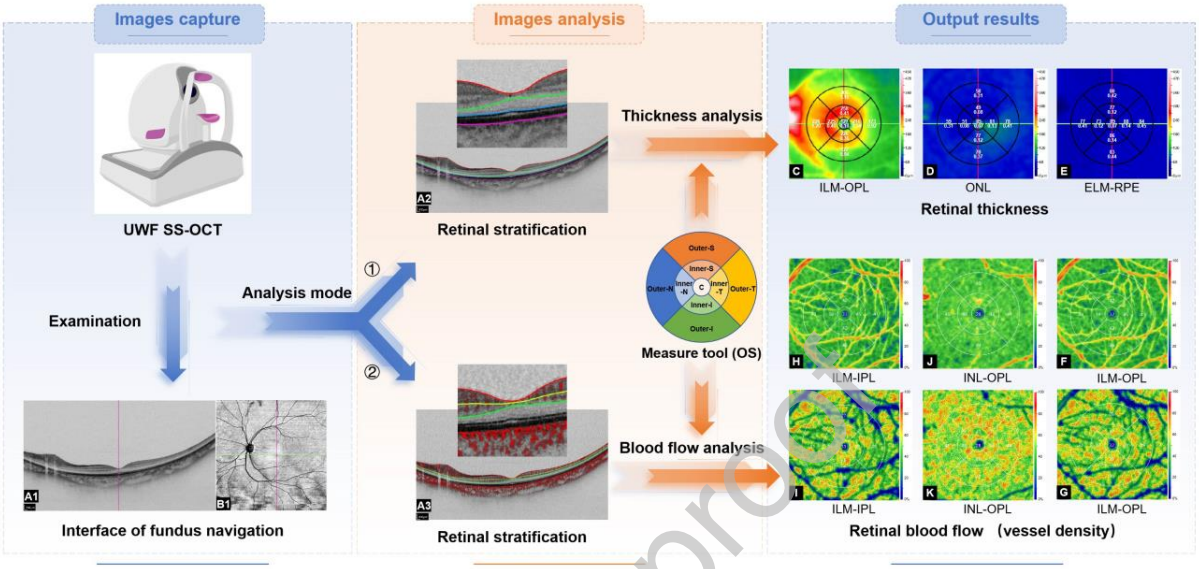


FIGURE CAPTIONS

FIGURE 1. Workflow of data analysis for retinal thickness and blood flow by UWF SS-OCTA.

(A1~3, B1) Fundus images for navigation. (C~E) Retinal thickness heatmap of IRLs, ONL and PL (μm). (F~G, H~I, J~K) Blood flow heatmap with and without large vessel of superficial capillary plexus (SCP), deep capillary plexus (DCP) and whole retina slab showed vessel density (%).

IRLs: inner retina layers, including layers inner limiting membrane (ILM) to outer plexiform layer (OPL). ONL: outer nuclear layer. PL: photoreceptor layer, including layers external limiting membrane (ELM) to retinal pigment epithelium (RPE).

Journal Pre-proof

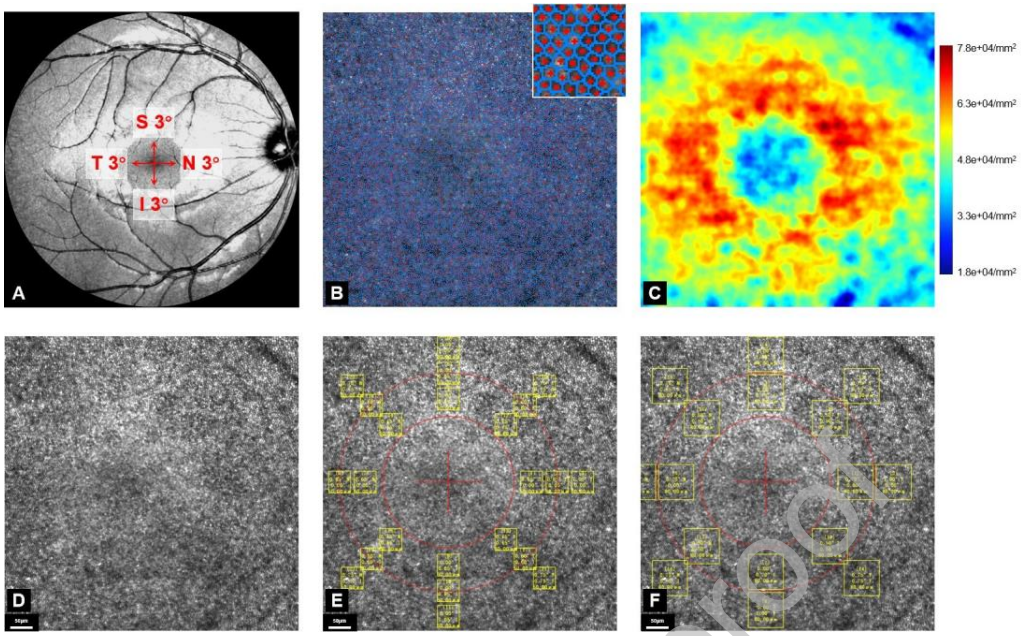


FIGURE 2. AO-SLO imaging and analytical results.

(A) Simulated navigation fundus demonstrating AO-SLO imaging at 3° eccentricity from the foveola. (B) Automated analysis of the cone mosaic showing segmented and counted cone photoreceptors (indicated by red dots, with each dot representing an individual cone). (C) Heatmap of cone density. (D) Cellular-level AO-SLO image of the cone photoreceptor mosaic. (E~F) Manual measurement with build-in tools in central images.

Journal Pre-proof

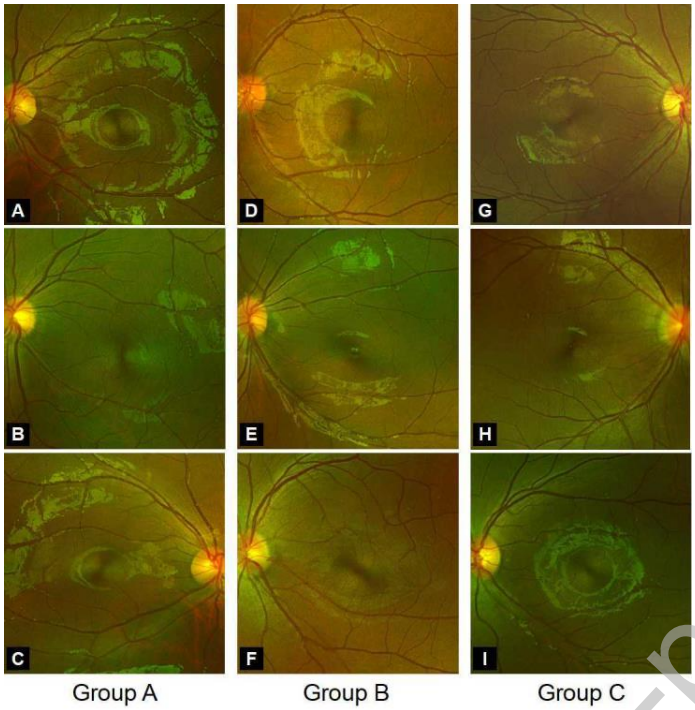


FIGURE 3. SLO imaging features of macular morphology.

(A~C) Eyes with low BCVA from FEVR and control groups (Group A). (D~F) FEVR-affected eyes with normal BCVA (Group B). (G~I) Healthy eyes with normal BCVA in control group (Group C).

Journal Pre-proof

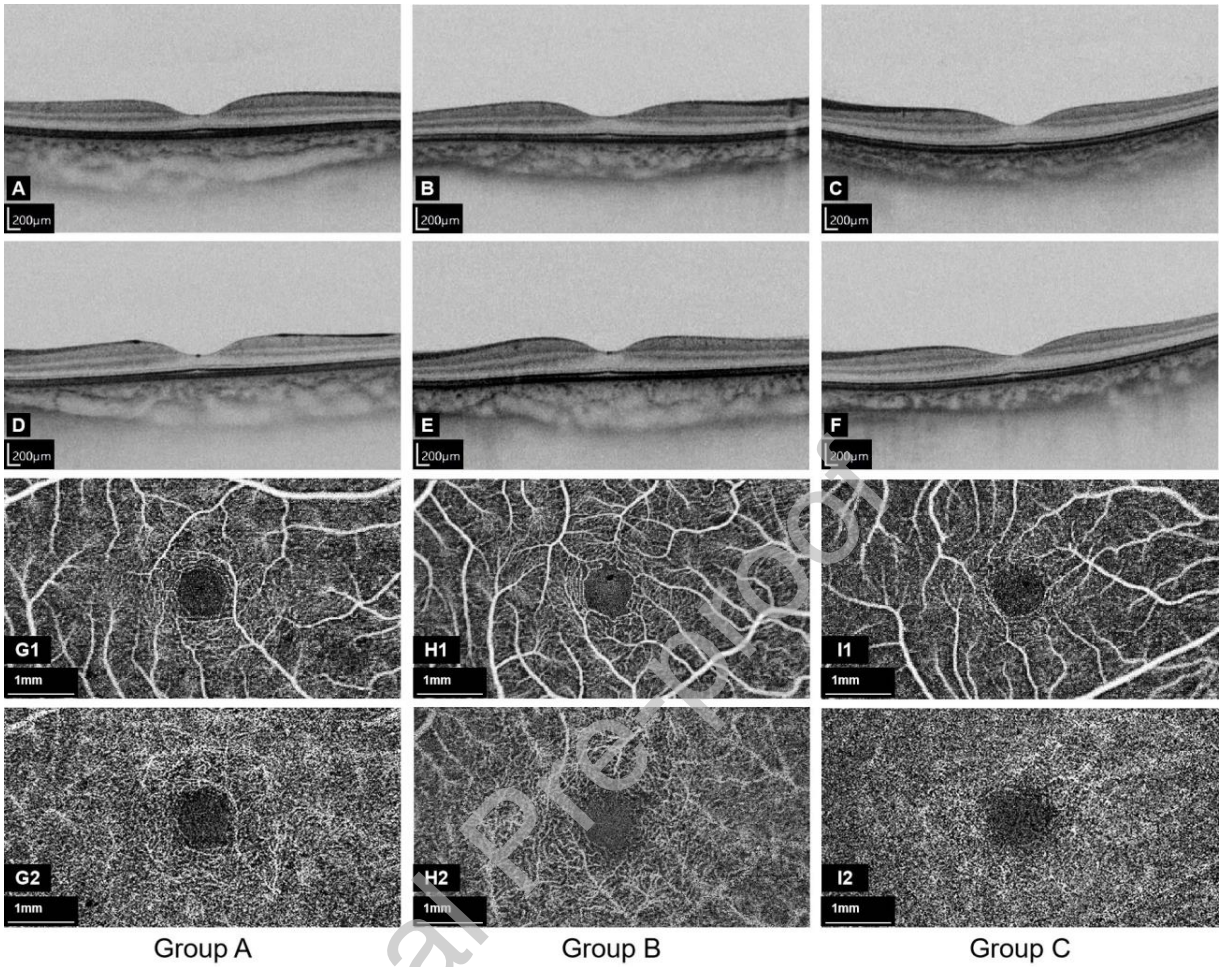


FIGURE 4. Macular Retinal Structure and Vasculature.

(A~F) Yransverse scan images of the macula. (G1~I1) Macular vascular images of SCP.

(G2~I2) Macular vascular images of DCP.

SCP: superficial capillary plexus. DCP: deep capillary plexus.

Journal Pre-proof

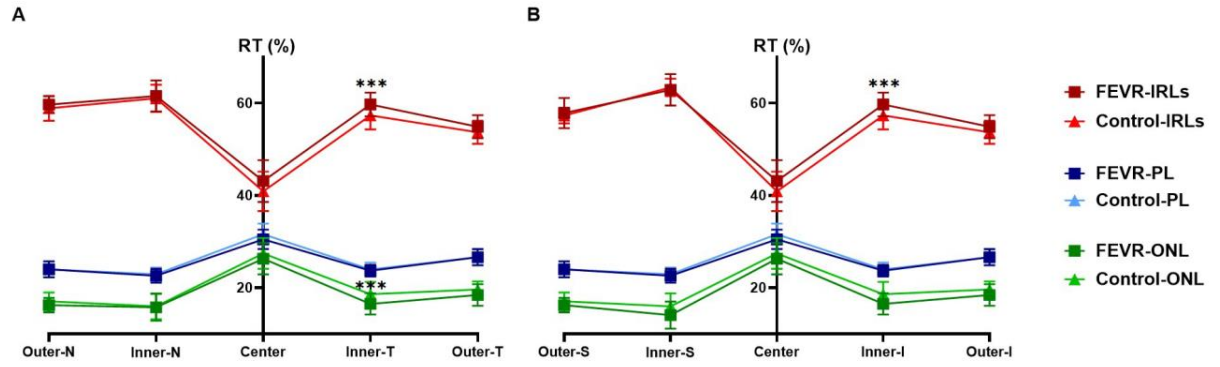


FIGURE 5. Comparison of retinal thickness in different layers between the FEVR and control groups.

(A) Plots showed retinal thickness of IRLs, ONL and PL at N and T positions between the two groups. (B) Plots showed retinal thickness of IRLs, ONL and PL at S and I positions between the two groups.

RT: retinal thickness. IRLs: inner retina layers, including layers inner limiting membrane (ILM) to outer plexiform layer (OPL). ONL: outer nuclear layer. PL: photoreceptor layer, including layers external limiting membrane (ELM) to retinal pigment epithelium (RPE).

Journal Pre-proof

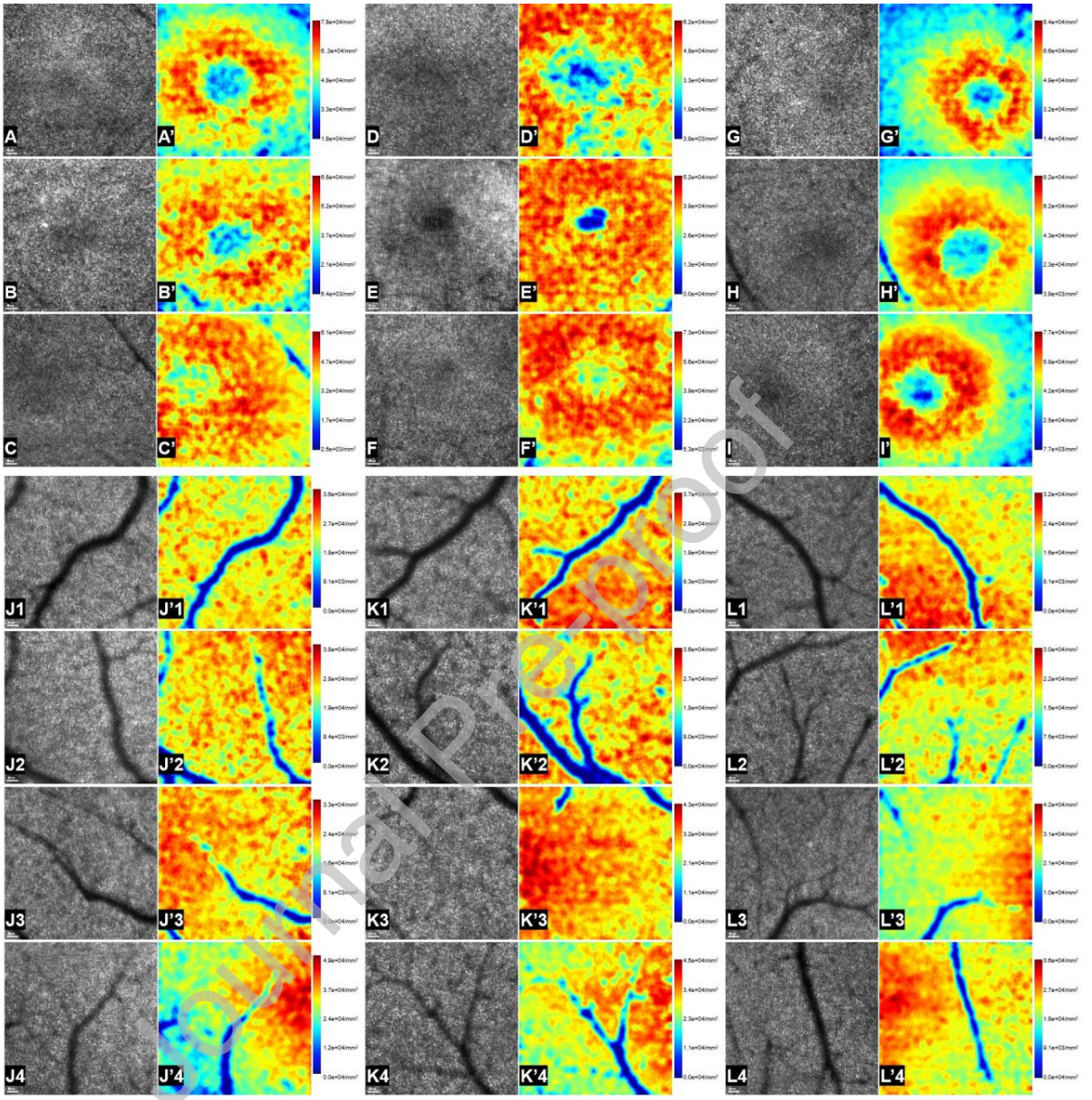


FIGURE 6. Foveal and parafoveal photoreceptor morphology and cone density heatmap.

(A~I) Central image of cone mosaic. (J/K/L1~4) Peripheral image of cone mosaic. (A'~I', J'/K'/L'1~4) Heatmap of cone density (Dark blue to dark red corresponds to increasing

cell density, and the value range varies in different images).

1~4: referred to the orientations of superior, inferior, nasal, and temporal in sequence.

TABLE 1. Basic characteristics of the participants.

Basic parameters	Participants (eyes)	Age	Gender (F/ M)	SE (D)	AL (mm)
All	32 (46)	9.76±5.28	24/22	-1.01±1.96	23.66±0.88
FEVR group	12 (15)	10.67±8.79	6/9	-1.83±2.42	23.86±0.98
Control group	20 (31)	9.32±2.29	18/13	-0.61±1.58	23.58±0.84
P*	NA	0.10[a]	0.25[b]	0.09[c]	0.30[a]
Participant A	left eye	7	Male	-1.75	24.36
Participant B	right eye	10	Male	+0.00	23.50
Participant C	right eye	6	Female	+2.50	21.61
Participant D	right eye	8	Female	-2.88	24.36

F: female. M: male. SE: spherical equivalent. AL: axial length.

Participant A~D (Group A): participants with low BCVA from FEVR and control groups.

[a] Mann-Whitney U test. [b] Pearson's chi-square test. [c] Independent samples t test.

* The comparison between FEVR and control groups.

TABLE 2. Comparison of the quantitative characteristics of macular fovea between the FEVR and control groups.

Foveal parameters	FEVR	Control	P
Retinal thickness of C IRLs (%)	43.15±4.53	40.92±4.26	0.16[a]

ONL (%)	26.33±3.42	27.46±3.33	0.35[a]
PL (%)	30.51±2.12	31.62±2.29	0.18[a]
R (μm)	286.46±19.22	276.38±22.76	0.19[a]
Retinal thickness of foveal center			
R (μm)	243.85±11.71	235.67±25.29	0.21[a]
FAZ area (mm^2)			
SCP	0.29±0.08	0.31±0.12	0.52[a]
DCP	0.55±0.21	0.42±0.16	0.11[b]
RCP	0.26±0.09	0.25±0.10	0.76[a]
FAZ perimeter (mm)			
SCP	2.25±0.38	2.36±0.51	0.50[a]
DCP	3.28±0.67	2.82±0.60	0.046[a]*
RCP	2.08±0.38	2.03±0.45	0.77[a]
Retinal vessel density of C			
SCP (%)	28.42±4.98	28.71±5.85	0.69[b]
DCP (%)	18.33±9.98	22.29±8.09	0.22[a]
RCP (%)	23.92±6.97	25.76±6.228	0.49[b]

C: center. IRLs: inner retina layers. ONL: outer nuclear layer. PL: photoreceptor layer. R: whole retina slab. FAZ: foveal avascular zone. SCP: superficial capillary plexus (ILM-IPL). DCP: deep capillary plexus (INL-OPL). RCP: capillary plexus of whole retina slab (ILM-OPL).

[a] Independent samples t test. [b] Mann-Whitney U test.

*P<0.05

TABLE 3. Comparison of retinal structure and vasculature around the macular fovea between the FEVR and control groups.

Retinal parameters	**FEVR**	**Control**	**P**	**FEVR**	**Control**	**P**

		Inner ring (1-3mm)			outer ring (3-6mm)		
S (%)							
RT	**IRLs**	62.91±3.40	63.44±1.91	0.94[a]	57.89±3.26	57.36±1.70	0.59[b]
	ONL	14.07±2.93	13.79±1.97	0.42[a]	16.57±1.83	17.11±1.29	0.32[b]
	PL	23.02±1.45	22.78±1.59	0.67[b]	25.54±2.26	25.53±1.49	0.99[b]
VD	**SCP**	31.77±3.52	32.00±3.59	0.97[a]	29.15±2.34	28.33±3.864	0.78[a]
	DCP	39.23±3.94	41.52±4.00	0.06[a]	41.77±2.74	43.14±1.96	0.04[a]*
	RCP	33.54±4.05	34.14±3.55	0.65[b]	29.62±3.31	28.95±3.69	0.53[a]
I (%)							
RT	**IRLs**	60.55±3.17	57.84±3.91	0.045[b]*	55.54±2.23	55.04±2.92	0.60[b]
	ONL	16.94±2.83	19.13±3.32	0.06[b]	18.17±2.17	19.07±2.07	0.24[b]
	PL	22.51±1.21	23.03±1.56	0.14[a]	26.28±2.23	25.88±1.68	0.56[b]
VD	**SCP**	32.31±2.21	30.05±4.47	0.20[a]	28.23±1.96	27.19±4.43	0.76[a]
	DCP	41.23±4.42	41.57±4.23	0.97[a]	40.31±3.50	39.81±6.62	0.63[a]
	RCP	33.69±3.17	32.52±4.57	0.43[b]	28.31±2.18	27.48±4.12	0.94[a]
N (%)							
RT	**IRLs**	61.59±3.36	61.07±2.95	0.61[a]	59.72±1.80	58.93±2.71	0.32[a]
	ONL	15.79±2.90	15.97±2.82	0.86[b]	16.24±1.57	17.09±1.92	0.19[b]
	PL	22.62±1.52	22.96±1.45	0.53[b]	24.03±1.75	23.98±1.71	0.88[a]
VD	**SCP**	31.31±2.90	32.19±4.07	0.25[a]	32.62±2.47	31.90±4.78	0.73[a]
	DCP	39.31±4.19	41.81±6.44	0.02[a]*	42.92±1.98	42.14±5.83	0.83[a]
	RCP	31.85±4.43	33.67±4.84	0.14[a]	32.62±3.10	31.43±4.61	0.92[a]
T (%)							
RT	**IRLs**	59.75±2.58	57.39±3.05	0.03[b]*	54.92±2.49	53.70±2.50	0.18[b]
	ONL	16.53±2.30	18.63±2.68	0.03[b]*	18.44±2.33	19.65±1.75	0.10[b]
	PL	23.72±1.28	23.98±1.50	0.25[a]	26.64±1.79	26.65±1.68	0.99[b]
VD	**SCP**	31.08±3.77	30.81±3.82	0.84[b]	26.69±2.32	26.10±3.99	0.96[a]
	DCP	40.46±4.48	43.57±3.19	0.07[a]	40.23±3.77	40.00±5.74	0.69[a]
	RCP	31.38±5.09	32.86±3.54	0.33[b]	28.54±2.03	27.81±3.39	0.80[a]

RT: retinal thickness. VD: vessel density. IRLs: inner retina layers. ONL: outer nuclear layer. PL: photoreceptor layer. SCP: superficial capillary plexus. DCP: deep capillary

Journal Pre-proof

plexus. RCP: capillary plexus of whole retina slab.

[a] Mann-Whitney U test. [b] Independent samples t test.

*P<0.05

TABLE 4. Comparison of the quantitative characteristics of foveal photoreceptors between the FEVR and control groups.

Quantitative parameters	FEVR	Control	P
Cone density (/mm^2)			
Inner-50	44416.25±4845.87	47592.37±6921.856	0.10[a]
Middle-50	46608.05±4808.11	49234.95±5361.43	0.13[a]
Outer-50	45526.23±5086.54	47339.24±4832.30	0.59[b]
Inner-80	45139.14±5000.19	48151.01±6207.86	0.13[a]
Outer-80	45660.56±5059.88	47533.06±4794.33	0.26[a]
Whole-300	42064.90±5277.38	43910.03±4143.57	0.23[a]
Cone spacing (μm)			
Inner-50	3.98±0.21	3.89±0.22	0.22[a]
Middle-50	4.00±0.23	3.95±0.17	0.40[a]
Outer-50	4.15±0.28	4.13±0.18	0.69[b]
Inner-80	3.96±0.20	3.89±0.19	0.23[a]
Outer-80	4.12±0.26	4.08±0.18	0.71[b]
Whole-300	4.19±0.26	4.14±0.16	0.52[a]
Cone dispersion (%)			
Inner-50	15.31±1.56	14.55±1.86	0.20[a]
Middle-50	13.40±2.30	12.46±1.98	0.18[a]
Outer-50	11.99±1.37	10.98±1.94	0.10[a]
Inner-80	14.26±1.65	13.68±1.72	0.31[a]
Outer-80	12.09±1.39	11.21±1.91	0.14[a]

Journal Pre-proof

Whole-300	14.43±1.42	13.81±0.94	0.11[a]
Cone regularity (%)			
Inner-50	95.86±0.97	95.96±0.88	0.74[a]
Middle-50	96.76±0.83	97.34±1.12	0.08[a]
Outer-50	97.45±1.04	98.18±1.16	0.03[b]*
Inner-80	95.98±0.78	96.30±0.90	0.27[a]
Outer-80	97.44±0.72	98.10±1.00	0.04[a]*
Whole-300	96.97±0.45	97.42±0.62	0.02[a]*

Inner/Middle/Outer-50: average value measured by 50μm tools. Inner/Outer-80: average value measured by 80μm tools. Whole-300: central image without a 300μm-diameter foveolar region.

[a] Independent samples t test. [b] Mann-Whitney U test.

*P<0.05

TABLE 5. Comparison of the quantitative characteristics of parafoveal photoreceptors between the FEVR and control groups.

Quantitative parameters	FEVR	Control	P
Cone density (/mm^2)			
S	24139.33±3199.54	20394.94±2422.79	0.002[a]*
I	24193.71±4275.18	20853.50±2403.44	0.02[a]*
N	25274.62±4100.93	22925.83±1935.53	0.08[a]
T	25388.51±3667.02	22894.12±2664.25	0.11[a]
Avg	24245.38±3421.74	21731.21±2393.68	0.03[a]*
Cone spacing (μm)			
S	5.27±0.42	5.90±0.45	0.002[a]*
I	5.25±0.51	5.77±0.43	0.008[a]*

N	5.31±0.41	5.57±0.24	0.049[a]*
T	5.24±0.35	5.63±0.39	0.04[a]*
Avg	5.33±0.40	5.69±0.42	0.02[a]*
Cone dispersion (%)			
S	18.01±1.27	17.21±2.53	0.30[a]
I	19.57±2.70	17.50±2.14	0.04[a]*
N	15.91±2.13	15.90±2.09	0.99[a]
T	17.22±2.12	15.25±2.03	0.06[a]
Avg	17.79±1.74	17.04±1.90	0.64[b]
Cone regularity (%)			
S	95.38±1.00	96.31±1.26	0.06[a]
I	95.20±1.23	96.02±1.37	0.13[a]
N	96.73±0.89	96.83±1.04	0.79[a]
T	96.47±0.76	97.16±1.16	0.06[b]
Avg	95.99±0.88	96.41±1.14	0.27[a]

S: superior. I: inferior. N: nasal. T: temporal. Avg: average.

[a] Independent samples t test. [b] Mann-Whitney U test.

*P<0.05

Table of Contents Statement:

Prospective multimodal imaging reveals: patients with mild familial exudative vitreoretinopathy exhibits characteristic partially thickening inner retina layers and thinning outer nuclear layer, irregular foveal avascular zone morphology, and cone density anomalies, showing no significant effect on visual acuity; participants with low vision but morphologically normal macular structure may also have underlying cone abnormalities. Cellular-level imaging supports exploring for microscopic phenotype and

potential pathogenesis. The findings could be identified as clinical biomarkers for diagnostic assistance.

Declaration of interests

☐The authors declare that they have no known competing financial interests or personal relationships that could have appeared to influence the work reported in this paper.

☒The authors declare the following financial interests/personal relationships which may be considered as potential competing interests:

Reports a relationship with that includes:. Has patent pending to. If there are other authors, they declare that they have no known competing financial interests or personal relationships that could have appeared to influence the work reported in this paper.

Journal Pre-proof